Desalination 476 (2020) 114219

Contents lists available at ScienceDirect

Desalination

journal homepage: www.elsevier.com/locate/desal

Small-scale desalination of seawater by shock electrodialysis

Mohammad A. Alkhadra[a,1], Tao Gao[a,1], Kameron M. Conforti[a], Huanhuan Tian[a], Martin Z. Bazant[a,b,*]

[a] Department of Chemical Engineering, Massachusetts Institute of Technology, Cambridge, MA 02139, USA
[b] Department of Mathematics, Massachusetts Institute of Technology, Cambridge, MA 02139, USA

GRAPHICAL ABSTRACT

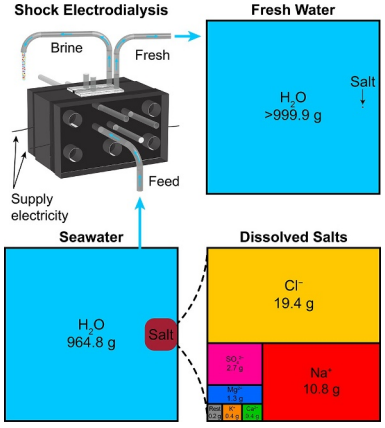

ARTICLE INFO

Keywords:
Shock electrodialysis
Seawater
Small-scale desalination
Selective separations
Electrokinetics

ABSTRACT

Conventional desalination technologies such as distillation and reverse osmosis are well suited for the supply of fresh water at large scale. The expensive infrastructure and high capital, operating, and maintenance costs associated with these technologies, however, limit their application in remote or underdeveloped areas. Here, we show that shock electrodialysis, a recently developed electrokinetic process, can be used to continuously desalinate artificial seawater (3.5 wt. %) for small-scale ($\leq$ 25 m^3 day^{-1} as a long-term goal), decentralized applications. In two steps, 99.8% of the salt fed was rejected, with selectivity for magnesium ions of which > 99.99% were removed (based on measurements of concentration by mass spectrometry). We also demonstrated for the first time the viability of using and continuously recycling solutions of sodium citrate buffer to simultaneously reduce waste and inhibit precipitation reactions in the electrode streams. As with conventional electrodialysis, the energy consumed by our technology can be significantly reduced by desalinating sources that are less saline than seawater, such as brackish water and various industrial or municipal process streams. Since the design of the system and choice of materials have yet to be optimized, there remain ample opportunities to further reduce the cost of desalination by shock electrodialysis.

* Corresponding author.
E-mail address: bazant@mit.edu (M.Z. Bazant).
URL: http://www.bazantgroup.mit.edu (M.Z. Bazant).
[1] Equal contribution.

https://doi.org/10.1016/j.desal.2019.114219
Received 13 September 2019; Received in revised form 8 November 2019; Accepted 12 November 2019
Available online 30 November 2019
0011-9164/

1. Introduction and background

Oceans represent the largest source of surface water and comprise roughly 97% of the total volume of water on Earth. Since these water bodies are salty, seawater is not directly a useful source of drinking water. The average salinity of seawater is approximately 3.5 wt. % (i.e., 35 g L^{-1}) [1], which means that every kilogram of seawater has about 35 g of dissolved salts. These salts include mainly sodium (Na^+) and chloride (Cl^-), but also magnesium (Mg^{2+}), calcium (Ca^{2+}), potassium (K^+), and sulfate (SO_4^{2-}). Although a costly endeavor, desalination of seawater is believed to be a promising solution to the globally increasing demand for fresh water. In 2016, the total production of fresh water worldwide via desalination was approximately 38 billion m^3, which is more than double the amount of production achieved in 2008 [2]. Processes for desalting seawater are typically driven by either thermal (e.g., distillation) or electrical (e.g., osmosis, solar, or wind) power. In this article, we use an emerging electrokinetic method known as shock electrodialysis (SED) to desalinate seawater. A potential advantage of SED over most other methods for continuous desalination is the ability to perform ionic separation, such as selective removal of multivalent ionic solutes. As a result of this selectivity, SED can be used to capture target species of high value. This technology also operates at ambient conditions and requires only enough pumping for fluidic transport through porous media, which precludes the need for high-temperature (distillation) or high-pressure (reverse osmosis, or RO) systems.

Historically, distillation (e.g., multi-stage flash and multiple-effect distillation) has been the method of choice for desalination of seawater, though more than half of the current desalination plants use RO in some capacity [3]. Distillation technologies, which are essentially sequences of heat exchangers, have high capital and energy costs, and are therefore mostly suitable in regions where the necessary fuel is affordable. RO, on the other hand, consumes much less energy and is therefore more efficient ($\approx$ 5 kWh m^{-3}) at desalinating seawater [4]. The governing principle of desalination using RO is to generate large enough pressures to overcome the osmotic pressure of seawater (up to 27 times atmospheric pressure) across a semi-permeable membrane. In a sense, RO removes water from the salt, irrespective of its concentration, which makes this technology less practical for decontamination (i.e., removal of trace toxic substances from water). RO also suffers from low water recovery during seawater desalination, such that the larger volumes of brine discharged come with high additional costs for disposal and environmental damage.

Another technology used for desalination is electrodialysis (ED), in which hydrated ions are forced through their respective ion-selective membranes by electrokinetic action. The advantage of this technology is that it does not involve phase changes (as in distillation) or conversion of energy from electrical to mechanical (as in RO). In electrodialysis, ions are directly transported by applying an electric field from a source of direct current. Once the region between these membranes becomes depleted of salt, however, the low conductivity of the solution will be compensated by an increased electric potential that ultimately drives up the energy requirement. This limitation has made electrodialysis impractical for processing feeds of less than 400 ppm of total dissolved salts [5].

A promising feature of SED is that it can continuously produce deionized ($\approx$ 10 μM) water, although the concentrations of the feed have only ranged from ~1 to ~100 mM of salt [6-8]. These previous experiments also involved only a single species of each charge (i.e., one cation and one anion) at a time. The goal of this study is therefore to examine the ability of SED to desalinate artificial seawater, in which we chose to include only the six most abundant components, namely Na^+, Mg^{2+}, Ca^{2+}, and K^+, as well as Cl^- and SO_4^{2-}. We based the composition of this model seawater on a technical report published by the US Department of Energy [1], a shown in Table 1. In our formulation, we excluded debris and large particulates such as sand, dirt, and seaweed to avoid clogging the device. (An SED system would in practice include a pre-filtration step to remove this suspended matter, which does not influence the energy demand of desalination.)

Table 1
Composition of artificial seawater based on the proportions of salt reported in the **Materials and experimental methods**. Concentrations are per unit volume of the solution. This formulation was motivated by data in a technical report published by the US Department of Energy [1]; these data (US DOE) are shown pictorially in the graphical abstract.

Species	Concentration & mass/mole fraction			
	g L^{-1}	[%]	mol L^{-1}	[%]
Sodium (Na^+)	11.178	[29.660]	0.486	[40.132]
Magnesium (Mg^{2+})	1.332	[3.533]	0.055	[4.522]
Calcium (Ca^{2+})	0.700	[1.859]	0.017	[1.433]
Potassium (K^+)	0.822	[2.181]	0.021	[1.735]
Chloride (Cl^-)	21.674	[57.514]	0.611	[50.467]
Sulfate (SO_4^{2-})	1.980	[5.253]	0.021	[1.701]
Total	37.685	[100]	1.211	[100]

2. Theory and operating principles

Although technologies for large-scale desalination have been extensively developed, little attention has been paid to the market of small-scale desalination, in which the capacity of water produced is less than 25 m^3 day^{-1}. Desalination at small scales, however, is a capability in high demand by industrial facilities, recreational and infrastructural spaces, development projects (both inland and coastal), health care and academic institutions, and military vessels [9]. This process, which demands low capital costs, capacities, and flow rates, could also serve isolated communities located in arid or remote regions as well as regions affected by natural disaster and armed conflict [10]. Advantages of desalination at small scales include decentralization of the water supply, low capital and construction costs, and low transportation costs by virtue of operating *in situ* [9]. Moreover, possession of a lightweight and portable device that is adaptable to the available sources of feed water offers flexibility in the types of problems that can be solved based on the unique needs of each sector. SED is a technology that is naturally operated at small scales, so it holds promise as a decentralized, point-of-use desalination system. Our current SED unit is a handheld device (~ $(3.7\ cm)^3$) that weighs 150 g (1/3 lbs, mostly from metal nuts and bolts) and can generate up to 0.5 L per day with little energy needed for fluidic pumping. When scaled up, this device can be designed to have dimensions similar to those of a 10.5-inch tablet computer (e.g., an Apple iPad which has dimensions of $1 \times 20 \times 25\ cm^3$) and to generate approximately 20 L per day with a pumping requirement similar to that of the current unit. This thin, rectangular geometry will facilitate parallelization of the system—for example by stacking several units on top of one another—to achieve the throughput desired for a small-scale application.

The first (batch) system to achieve deionization by SED in the laboratory was designed, built, tested, and patented by our group [6, 7, 11, 12]. Recent generations of this system [8, 13] involve a cross-flow architecture that enables continuous operation, whereby feed flows into a microporous glass frit (a weakly charged medium with small pores) positioned between identical cation exchange membranes, as shown in Fig. 1. The process of SED requires formation of a sharp gradient—a shock wave—in the concentration of ions in the frit [14, 15], which is accomplished by applying an electric field that drives cations out of the "deionized" region. For the system to maintain bulk electroneutrality, anions leave this region in the opposite direction (toward the anode) because they would otherwise be blocked by the ion-selective membrane. This so-called concentration polarization [14] leads to enrichment of ions near the anode as well as depletion near the cathode. As

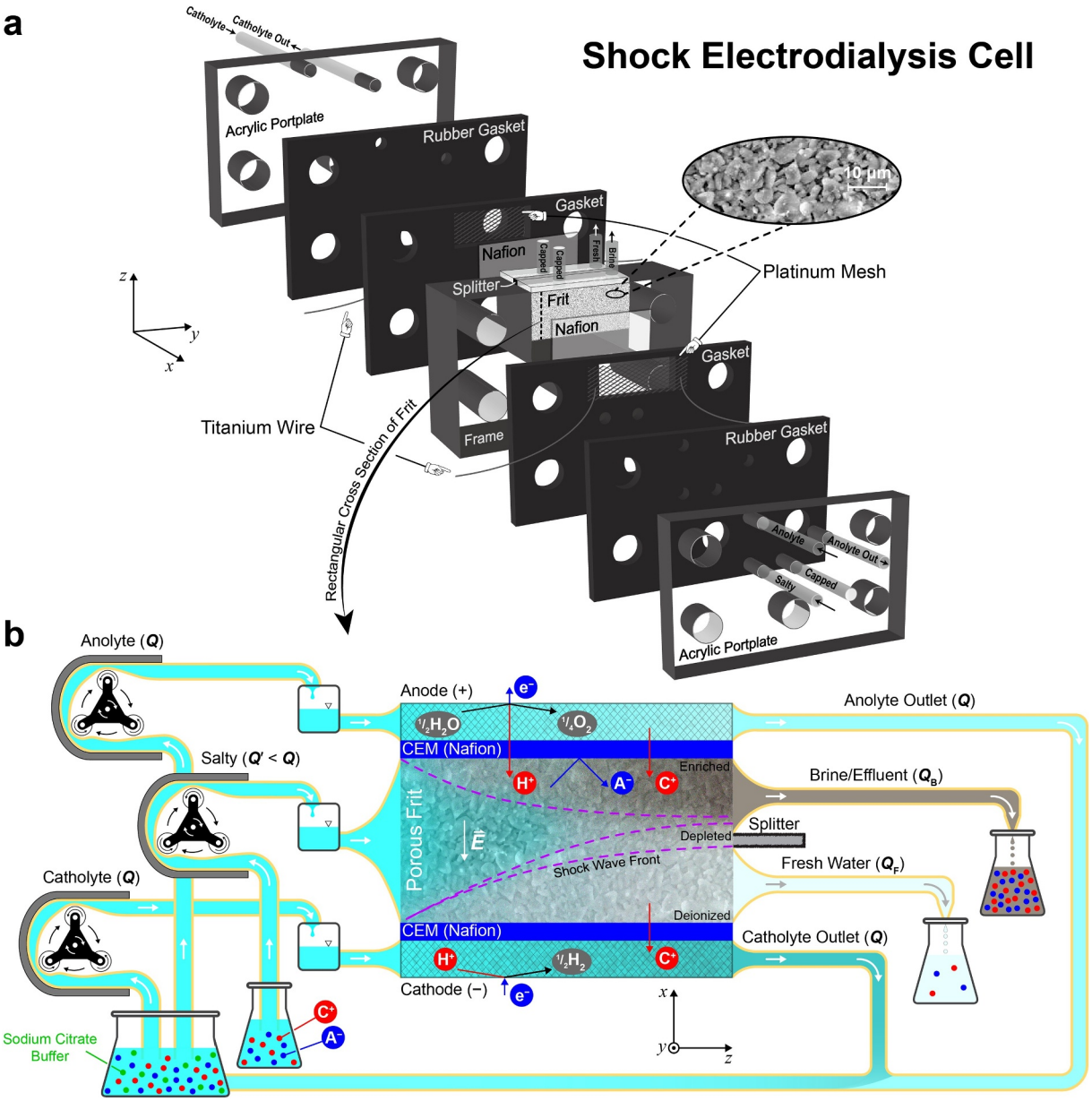

Fig. 1. Schematic of the SED device that demonstrates both assembly and operating principles. (a) A working device consists of platinum electrodes, titanium wire, and a microporous borosilicate frit sandwiched between identical nafion membranes which permit passage of only cations. The inlet (outlet) streams are labeled *contaminated*, *anolyte* (*anolyte out*), and *catholyte* (*catholyte out*); fluid leaving the top edge of the frit is split into *fresh* and *brine* streams. The close-up image of a glass frit taken by scanning electron microscopy was reproduced with permission from Deng et al. *Langmuir* 2013, 29, 16167–16177. Copyright 2013, American Chemical Society. (b) A rectangular cross section of the frit shows water splitting at the anode and formation of molecular hydrogen at the cathode, which are the primary electrochemical reactions that provide current to the cell. Contaminated water in the frit is then subjected to an external electric field ($\vec{E}$) that transports charged species perpendicular to the flow. In (b), flow rate is denoted by the letter ***Q***, and streams are colored based on relative concentration.

ions are depleted in the deionized region, the system will tend to its diffusion limited current at which the rate of ion transport is constrained by how fast analyte can diffuse to or from the electrodes. The weakly charged surfaces of the frit, however, are able to support the electrolyte by providing "overlimiting conductance," which ultimately leads to the separation of ions into enriched and depleted zones [14]. Physically, these zones are separated by a propagating deionization shock wave in the porous medium [15], similar to the concentration shocks first observed in microfluidic devices [16-18]. This electrokinetic separation can be made continuous by driving flow (through the frit) perpendicular to the applied electric field [7, 8]. A physical splitter placed at the outlet is then used to collect each of the enriched and deionized streams.

The primary mechanisms of overlimiting conductance include surface conduction, which dominates in thin channels (~ 1 μm), and surface convection (i.e., electroosmosis), which becomes important in larger channels (~ 100 μm) [14]. Surface conduction is driven by excess counterions (in this case cations) that screen the (negative) charge of the walls and amplify the axial electric field in the depleted region, where bulk conductivity is reduced [15]. This amplified electric field then forces coions (in this case anions) out of the depleted region (in the positive *x*–direction), which sharpens the concentration gradient and concomitantly produces a steady shock wave. As the width of pores is increased, surface convection by electroosmotic flow overpowers surface conduction as the dominant mechanism of overlimiting conductance [14, 18]. In our system, electroosmosis also propels the

electrolyte in the direction of applied electric field (negative x–direction), such that the fraction of deionized water recovered is automatically increased at high currents [8].

3. Materials and experimental methods

The device used here was fabricated according to a design recently published by our group [13]. This continuous, laboratory scale architecture is shown schematically in Fig. 1. The device comprised 3 inlets and 4 outlets: 2 of the inlets transported fluid to the electrodes and the third delivered contaminated feed; 2 of the outlets transported fluid from the electrodes and the other 2 were generated at the splitter as fresh and brine streams. To eliminate acid dosing of the cathode stream (done in previous studies [13, 19] with HCl to inhibit precipitation of metal hydroxides), we used solutions of sodium citrate buffer for both electrode streams which were continuously recycled during the process (closed-loop operation). The electrodes were platinum meshes (Sigma–Aldrich) connected to a Gamry Reference 3000™ potentiostat/galvanostat using titanium wires (Alfa Aesar), the cation exchange membranes were nafion N115 (with dimensions of approximately 127 μm × 1 cm × 2 cm), and the porous medium was a borosilicate frit (with dimensions of approximately 3 mm × 2 cm × 1 cm). The frit (Adams & Chittenden Scientific Glass) had ultrafine pores (nominally ranging from 0.9 to 1.4 μm in size), an internal surface area of 1.75 $m^2 g^{-1}$ based on Brunauer–Emmett–Teller (BET) theory, a mass density of 1.02 g m^{-3}, and a porosity of 0.31. Before assembling the device, the frit was glued onto an acrylic frame using Devcon 2 Ton Epoxy (McMaster-Carr). The splitter, placed midway down the frit for ease of assembly, was made of cast acrylic and was sealed against the top face of the frit using 0.04-inch GORE™ expanded polytetrafluoroethylene (ePTFE) gasket tape. Holes in all of the acrylic slabs and rubber gaskets were created using a laser cutter (Universal Laser Systems) and refined with a drill press (Palmgren 10-inch, 5-speed bench model). These layers were then stacked and held together with nuts, bolts, and washers made of 316 stainless steel.

To prepare artificial seawater with the composition reported in Table 1, we added 27.22 ± 0.01 g of sodium chloride (NaCl), 3.29 ± 0.01 g of sodium sulfate decahydrate ($Na_2SO_4 \cdot 10H_2O$), 11.13 ± 0.01 g of magnesium chloride hexahydrate ($MgCl_2 \cdot 6H_2O$), 2.56 ± 0.01 g of calcium chloride dihydrate ($CaCl_2 \cdot 2H_2O$), and 1.85 ± 0.01 g of potassium sulfate (K_2SO_4) for every liter of deionized water. This solution was fed to the device solely through the stream labeled “salty” (see Fig. 1) for desalination. The electrode streams, on the other hand, drew from a solution of sodium citrate buffer that was continuously recycled. The purpose of using such a solution (as opposed to acid dosing of the catholyte) was to reduce waste by recycling the electrode streams, inhibit precipitation reactions, and prevent undesired side reactions like the evolution of chlorine gas. In this study, we chose sodium citrate because it buffers in the relevant range of pH ($\sim 4-7$) to prevent scaling (i.e., formation of $Mg(OH)_2$ and $CaCO_3$), it does not react with the cations in seawater, and it is stable at the redox potentials in the cell [19]. To prepare the buffer, we first formulated a solution of citric acid ($HOC(COOH)(CH_2COOH)_2$) and its conjugated base sodium citrate dihydrate ($HOC(COONa)(CH_2COONa)_2 \cdot 2H_2O$) with concentrations of 0.5 M each in deionized water. The pH of this mixture was measured to be approximately 4.0 and was adjusted to a final pH of 4.9 by adding an appropriate volume of sodium hydroxide (1 M). (All reagents were purchased from Sigma–Aldrich and used as received.) During operation, the buffer would become slightly more acidic in the anolyte and slightly more alkaline in the catholyte, but as these streams were mixed, the buffer recovered its starting pH and buffering capacity. Moreover, the (anionic) conjugate base of the buffer was confined to the electrode streams because they were separated from the frit by cation exchange membranes. Confinement of the conjugate base to these streams was what allowed the buffer to maintain its pH and buffering capacity under closed-loop operation.

With these solutions prepared, we began our experiments by setting the flow rates of all streams. In this work, all flow rates were held constant: 0.021 ± 0.002 mL min^{-1} for the salty feed and 0.27 ± 0.01 mL min^{-1} for the electrode streams. The cross-sectional area of the frit through which liquid flowed had an area of 3 mm × 2 cm = 0.6 cm^2, and so the superficial velocity of the salty feed was 5.8 ± 0.6 μm s^{-1}. This flow rate of the feed was chosen to keep the diffusion limited current (see **Results and discussion**), and in turn operating voltage, low. The flow rate of the electrode streams was then chosen to be an order of magnitude greater to impose enough pressure on the nafion and prevent salty feed from bypassing the frit. To transport all liquids, we used peristaltic pumps equipped with Tygon® Chemical tubing (Saint-Gobain). With such pumps—and at low speeds of rotation—the flow would be pulsed, though it was made smooth by incorporating hydraulic accumulators just upstream of the device. In our system, the accumulators were capped glass vials that held a small volume of (compressible) air above the (incompressible) liquids being pumped at the bottom to smooth out pulsations. With flow rates set and tubing connected, the accumulators were left to pressurize and the system to equilibrate overnight, after which the Gamry was set to operate galvanostatically. (Air inside the accumulators became pressurized over time until the fluidic resistance downstream—such as that created by the porous frit—was overcome by the pumped liquid.) The measured voltage was allowed to stabilize for at least 1 h until it reached steady state.

Samples were collected approximately every 3 h at each dimensionless current directly from the device and stored in conical centrifuge tubes for analysis. Empirical analyses included measurement of volume, conductivity, pH, and concentration of cations. Conductivity and pH were measured using Mettler Toledo analytical instruments (SevenCompact pH/Cond S213), and concentration was determined by inductively coupled plasma mass spectrometry (Agilent 7900 ICP–MS). The plasma in ICP–MS was made from argon gas and was supplemented by helium. To improve the accuracy of our data and subsequent analysis, we incorporated an internal standard that introduced 100 ppb of indium to all samples. Since the output of ICP–MS was in counts per second, quantitative analysis required calibration of the measurements. A calibration curve was produced by linear regression of reference standards with known concentration. These calibration standards (Na, Mg, Ca, K, and In) were purchased from Sigma–Aldrich and serially diluted to prepare a set of samples that encompassed the concentrations relevant to this study. For concentration to fall within the detection limits of the spectrometer and to avoid damaging the detector, all samples and standard solutions were diluted in nitric acid to a final acid composition of 2 vol. %. To calculate the true concentration of a solution, concentrations found from calibration curves were multiplied by the corresponding dilution factor used to prepare the sample.

4. Results and discussion

Propagation of a shock wave across which concentration varies sharply is the key phenomenon that governs deionization in SED. This shock—as well as the depletion zone beneath it—is generated by applying current in excess of the diffusion limited current (I_{lim}), which is defined as the rate of forced convection of positive charge carriers:

$$I_{lim} = \sum_j \nu_j C_j F Q' \tag{1}$$

where ν is valence (charge), C is molar concentration, F is Faraday's constant, Q' is the volumetric flow rate of the feed, and the sum is taken over all cations j. In the presence of ideal cation exchange membranes, the flux of anions is 0 at steady state (assuming that these species do not participate in chemical reactions). Using the composition of artificial seawater in Table 1 and with $Q' = 0.025$ mL min^{-1}, we find that

$$I_{lim} = 2.43 \times 10^{-2} \quad \text{A} \tag{2}$$

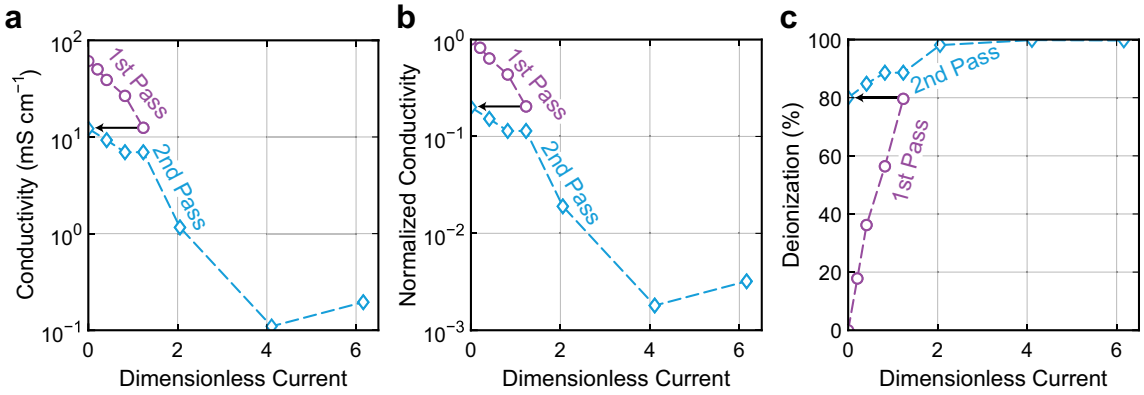

Fig. 2. Quantitative analysis of (artificial) seawater desalination in a 2-step process. Measurements of (a) absolute and (b) normalized conductivity of the fresh stream; in (b), conductivity is normalized relative to that of the feed to the first pass (composition outlined in Table 1). (c) Deionization of the fresh stream calculated based on Eq. (3). The feed to the second pass (I_{lim} = 4.86 mA) was a 5-fold dilution of the feed to the first (I_{lim} = 24.3 mA).

After exceeding I_{lim}, the overlimiting current increases linearly with voltage and effects constant conductance, which is consistent with the governing theory as well as previous experimental observations in negatively charged porous media [7, 14].

Since applying a constant (overlimiting) current facilitates the formation of a stable deionization shock [8], we operated our SED system galvanostatically. (Potentiostatic operation, on the other hand, may lead to overshoot and oscillation about a desired overlimiting current, which could generate variable or perhaps unstable shocks [17].) To quantify the performance of SED for desalination of seawater, we measured the conductivity of the fresh stream, as shown in the leftmost panel of Fig. 2. Based on the observed level of desalination (≈ 80% in the first pass), we conclude that 2 distinct zones of concentration polarization are established above and below a deionization shock, despite the high ionic strength (≈ 750 mM) of seawater. This high concentration of ions, however, corresponds to a relatively large limiting current, which when multiplied by the steady voltage produces a high power demand. In practice, the energy consumption of common desalination technologies (e.g., distillation and RO) is lowered by using multiple stages serially [20, 21]. This approach is particularly suitable for SED because power scales quadratically with current in the overlimiting regime, with voltages on the order of 1 to 10 V. (At voltages a few times the thermal voltage of 26 mV at 300 K, $I \sim V$ [14] so that $P = IV \sim I^2$.) Operating the system in a sequence of passes, each at a lower current than for a one-step process, would therefore reduce power consumption, though at the expense of water recovery.

4.1. Desalination performance

We proceeded to desalinate artificial seawater in a 2-step process that we accelerated (to compensate for low throughput) by feeding serially diluted solutions in turn to the same device. A dilution factor of 5 was chosen for the second step based on the reduction of conductivity in the first at 1.2 times the limiting current (arrows in Fig. 2). In other words, concentrations of the feed to each pass were 35 g L^{-1} (1.1 M; I_{lim} = 24.3 mA) and 7 g L^{-1} (0.22 M; I_{lim} = 4.86 mA). Our results for desalination of artificial seawater in 2 passes are presented in Fig. 2, where deionization (the percentage removed of a given species, *DI*) is defined as

$$DI = 100\% \times \left(1 - \frac{C_{fresh}}{C_{feed}}\right) \tag{3}$$

and dimensionless current ($\tilde{I}$) as $\tilde{I} = I/I_{lim}$. From Fig. 2b, SED reduces the conductivity of artificial seawater by 3 orders of magnitude in 2 passes. This reduction in conductivity corresponds to 99.8% desalination under the optimal conditions tested: 79.6% in the first pass with $\tilde{I} \approx 1.2$, and 99.1% in the second with $\tilde{I} \approx 4.1$. Purification to this extent brings the artificial seawater to a salinity of 67.8 ppm, well below the recommended upper limit of total dissolved solids in drinking water [22].

Measurement of desalination by conductivity alone narrows the scope of our analysis because it precludes the ability to examine the fate of individual ions. Moreover, changes in conductivity of the fresh stream are influenced by production (and transport) of hydronium and hydroxide from self-ionization of water. We therefore used ICP–MS as a more precise measure of composition to rigorously characterize deionization. The results of this analysis are presented in Fig. 3, which demonstrate that the concentration of Na^+ decreased by approximately 80% in the first pass, as indicated by a red arrow in the top row of panels. (The concentrations of the other cations did not match exactly between passes because the feed to the second pass was a 5-fold dilution of the entire solution, rather than a new solution with one-fifth the composition of each ion.) And since Na^+ was the most abundant cation in the electrolyte, we attributed the decrease in conductivity by 80% in the first pass (Fig. 2) to removal of this species, even though all other cations were removed to a greater extent.

4.2. Ionic selectivity

The other important aspect revealed in Fig. 3 is selective removal of certain ions over others: in the second pass, Mg^{2+} is preferentially removed relative to all other species by at least one (Mg^{2+}:K^+) and up to nearly two orders of magnitude (Mg^{2+}:Ca^{2+}). For a more quantitative analysis of this observation, we used the data in Fig. 3 to calculate scaled (retention) selectivity in the fresh stream as a function of dimensionless current between each pair of unique species. In this context, scaled selectivity is defined as [13]

$$S_{j:i} \equiv j{:}\ i = \frac{C_i/C_j}{C_{i_0}/C_{j_0}} = \frac{C_i/C_{i_0}}{C_j/C_{j_0}} \tag{4}$$

which may be interpreted as the ratio of the effluent concentration of species *i* to that of species *j*, scaled by the corresponding ratio of feed concentrations (which is also equal to the ratio of normalized effluent concentrations). If $S_{j:i}$ is greater than 1, then species *j* is selectively removed relative to species *i*. An experimental paper recently published by our group demonstrated that SED automatically achieves selective removal of the multivalent ion from an electrolyte comprising Na^+ and Mg^{2+} in various proportions. In that article, selectivity based on valence was attributed to differences in ionic mobility across the enriched and deionized regions of the device in the regime of overlimiting current [13].

In this study, the electrolyte consisted of four primary cations, two

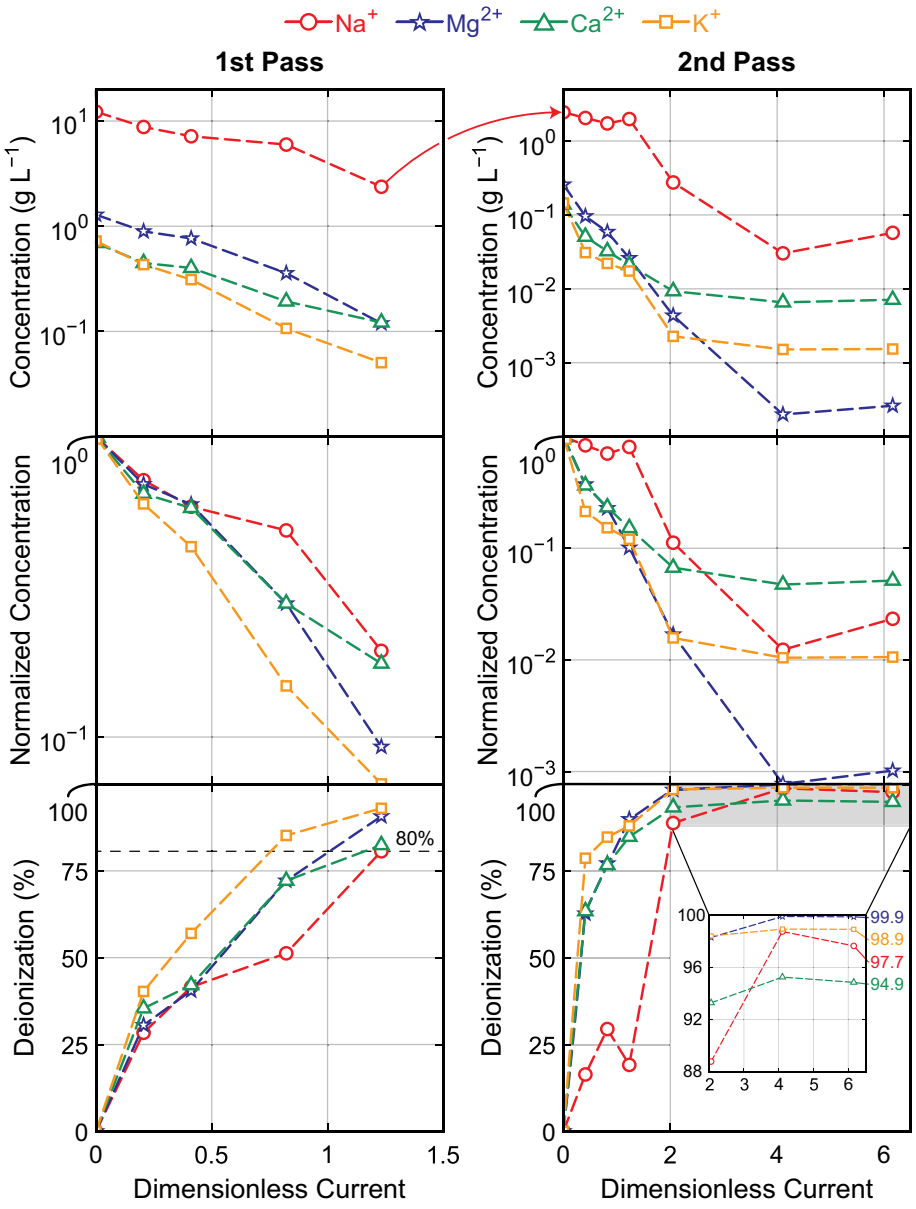

Fig. 3. Quantitative analysis of (artificial) seawater desalination in the 2-step process using ICP–MS. Measurements of (top) absolute and (middle) normalized concentration of cations in the fresh stream; in the latter, concentration (of each ion) is normalized relative to that of the feed to each respective pass (composition outlined in Table 1). (Bottom) Deionization of the fresh stream calculated using Eq. (3). Note that the feed to the second pass was a 5-fold dilution of the entire solution, rather than a new solution with one-fifth the composition of each ion.

of which are monovalent and the other two divalent. The left panel of Fig. 4 shows that there was only modest selectivity of certain ions relative to others in the first pass. This behavior was likely because we operated the system at or below the limiting current, which precluded formation of a deionization shock sustained by overlimiting conductance. The right panel of Fig. 4, on the other hand, indicates that there was significant selectivity of Mg^{2+} relative to all other species in the second pass when overlimiting current was applied. Removal of this ion is an important and desirable capability in the inhibition of magnesium-based (mineral) scale, in which Mg^{2+} forms insoluble salts that precipitate, deposit on surfaces, and impair the performance of desalination units [23]. In this regard, our experiments show that SED has the potential to soften seawater without the need for antiscalants.

Although we expect that multivalent ions should typically be removed more effectively compared to monovalent ions [13, 19], the behavior of Ca^{2+} goes against this intuition in the second pass when overlimiting current is applied (in Fig. 4, Ca^{2+}:Na^{+} and Ca^{2+}:K^{+} are both less than 1 at high current). A possible reason for this lack of selectivity may be reaction of Ca^{2+} to form uncharged species that evade removal by SED. For example, Ca^{2+} can react with bicarbonate [24] (HCO_3^-, which is produced by dissolution of carbon dioxide in water) according to the chemical reaction

$$Ca^{2+}(aq) + 2HCO_3^-(aq) \longrightarrow CaCO_3(s) + CO_2(g) + H_2O(l) \quad (5)$$

This reaction more readily occurs under alkaline conditions, which was the case in the second pass at high current (e.g., pH = 9.72 at $\tilde{I} = 6$ versus pH = 4.65 at $\tilde{I} = 0.4$). Moreover, since the pH of the desalted stream was only slightly basic, the reaction of Mg^{2+} with hydroxide (OH^-) was negligible, which ensured that magnesium remained charged and amenable to electrokinetic separation. (We estimate that $Mg(OH)_2$ will precipitate from solution when the pH exceeds 10.6 for a concentration of Mg^{2+} of 10^{-3} g L^{-1}, or 0.04 mM, and assuming a solubility product constant of 5.61×10^{-12} [25].) Practically, it is

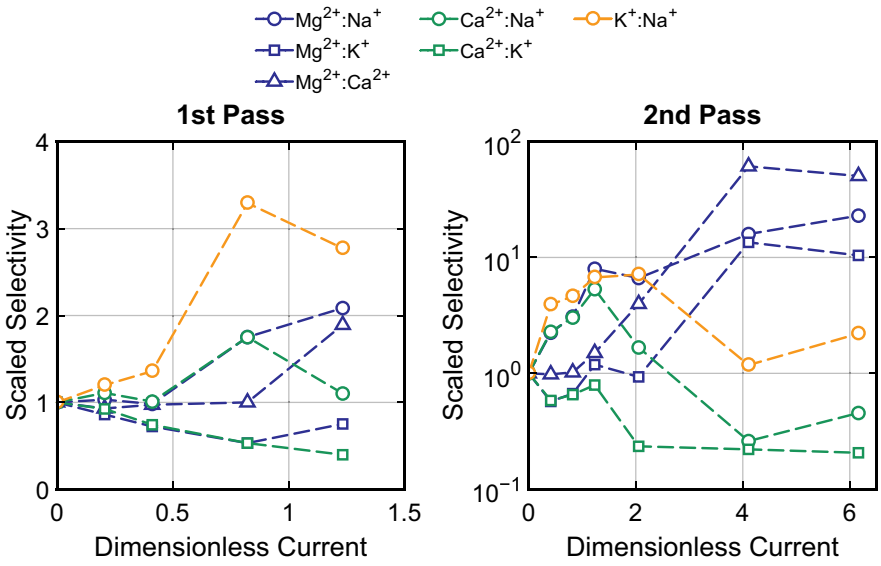

Fig. 4. Quantification of the selective removal of ions in the 2-step desalination process. Graphs show scaled selectivity ($S_{j:i} \equiv j:i$) for each pair of unique species in the fresh stream as a function of dimensionless current in each pass. Values of $S_{j:i}$ are calculated using Eq. (4) based on the normalized concentrations in Fig. 3.

more desirable to remove Mg^{2+} than Ca^{2+} from seawater because the former is 5 times more abundant (in molar units) [1] and as a result generates more mineral scale.

A subtle feature of Fig. 4 is the selective removal of all species relative to Na^+ in the second pass at or below the limiting current. This behavior may be due to inhibited removal of Na^+ from the feed because of the high concentration of this species in the electrode streams (34.5 g L^{-1}, or ~ 1.50 M, in the buffer solution). In other words, it is likely that there exists a driving force—established by gradients in the concentration of Na^+—that balances the Coulomb force induced at or below the limiting current. This observation would also explain the comparatively poor removal of Na^+ in the second pass at low current in Fig. 3.

4.3. Water recovery and energy demand

Aside from deionization, water recovery and energy efficiency are important metrics in desalination systems, and so we analyze the recovery ability and energy demand of SED when used to desalt artificial seawater. Water recovery (*WR*), sometimes referred to the recovery ratio, is defined as

$$WR = \frac{Q_F}{Q'} \tag{6}$$

where Q_F is the volumetric flow rate of the fresh stream and Q' is the volumetric flow rate of the feed; *WR* is shown in Fig. 5a to increase (up to 70% in the second pass) with current. In general, this increase in water recovery is strictly due to electroosmosis in the direction of applied electric field, which automatically delivers more fluid to the deionized region [8] ; the splitter was not repositioned in this experiment. Since the electrode streams are continuously recycled under closed-loop operation, the only waste that is generated by our device (and has to be disposed of) is the concentrated brine stream. And if the system is operated at a dimensionless current of 4, then only 0.5 m^3 of brine is generated for every 1 m^3 of desalinated water in the second pass. In future iterations of our device, water recovery will be increased by adjusting the position of the splitter to favor a larger flow rate of fresh water.

Analysis of the electrical power needed for deionization is reported in Fig. 5b & c; power is calculated as the product of applied current and (steady) voltage, and energy density as power divided by the volumetric flow rate of the feed. In desalinating seawater, power (and thus energy density) increases quadratically with current in agreement with the governing theory [14]. Moreover, Fig. 5 b & c reveals that the overall energy demand of SED is higher than that of more established desalination technologies like RO [26] and ED [27]. This comparison indicates that SED is still in its early stages of development and may not be the preferred method of desalination. Fig. 5 b & c also shows,

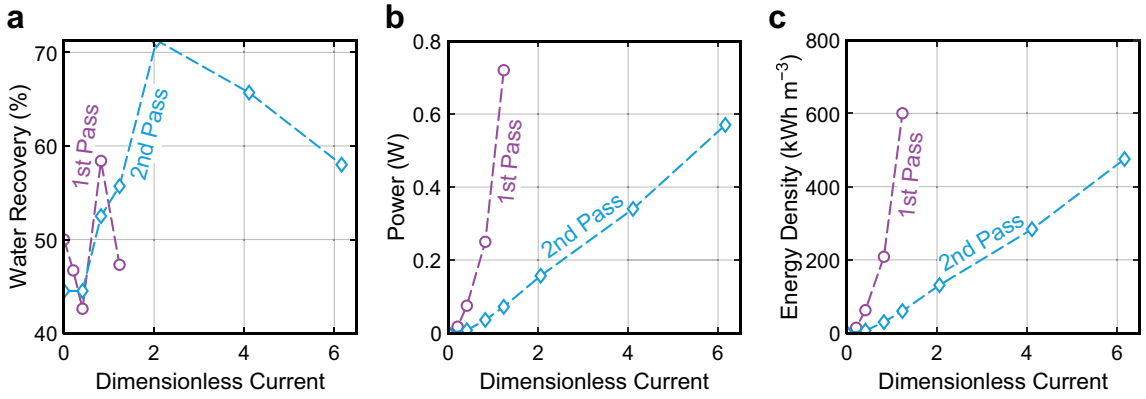

Fig. 5. Analysis of water recovery and energy demand in the 2-step process of seawater desalination. (a) Water recovery as a function of dimensionless current in each pass. (b) Power and (c) energy density as functions of dimensionless current in each pass.

however, that the energy requirement drops significantly as the solution fed becomes more dilute. These observations (supported by the dependence of limiting current on concentration in Eq. (1)) imply that the energy consumption of SED can be significantly reduced by desalinating sources that are less saline than seawater, such as brackish water. (Although energy consumption is reduced in general by treating dilute feeds—even for physical methods such as distillation and RO—this effect is more prominent in the dilute limit for electrochemical methods such as SED [7, 8], ED, or capacitive deionization [28] because ions are removed rather than the water.) We also note that the cost of fluidic pumping in our current laboratory scale system is negligible compared to the cost of electrical energy. (The power needed for pumping is $P_{\text{pump}} = Q\Delta p$, where Δp is pressure drop and was approximately 2 psi across the frit and 1 psi across each electrode.) The cost of pumping will become important at larger scales, however, and it will increase according to the desired level of throughput.

To lower the energy requirement and improve efficiency, our SED technology can be optimized most directly by modulating the geometry of the frit. By simple scaling arguments, power is calculated as $P = IV$ and Ohm's law states that $V = IR$, so $P = I^2R \sim Q^2L/A$ (L is the length of the resistive material and A is its cross-sectional area) for fixed dimensionless current ($I_{\text{lim}} \sim Q$) and assuming fixed resistivity of the electrolyte. Energy density is then $\hat{E} = P/Q \sim QL/A$ and may therefore be reduced by increasing the cross-sectional area of the frit, which in Fig. 1 corresponds to the y– and z–dimensions. The only disadvantage of increasing the z–dimension—the direction of fluid flow—would be larger hydrodynamic resistance and in turn greater cost of pumping, although the magnitude of this cost would remain small. Otherwise, increasing cross-sectional area will enable more throughput as well as parallelization of the system, for instance by stacking several units on top of one another. Scaling up the system in this way will also improve the performance of SED by increasing the distance over which the shock wave propagates (in the z–dimension) and in turn requiring a smaller overlimiting current to achieve the same degree of desalination.

5. Conclusion

Although technologies for large-scale desalination have been extensively studied and optimized, specialized systems for small-scale desalination are underexplored. Motivated to address this shortcoming, we used SED to continuously desalinate artificial seawater and observed selective removal of Mg^{2+} relative to all other cations present. In 2-steps, 99.8% of the salt fed was rejected, with more than 99.99% of Mg^{2+} removed. SED has several unique and attractive features that make it suitable for small-scale and decentralized desalination. In particular, our system is robust, lightweight, and portable, and it may be redesigned in such a way that will facilitate scale-up and parallelization for greater throughput. Moreover, we have shown by scaling arguments that scale-up can reduce power consumption while retaining the high performance demonstrated in this article. Finally, we reported for the first time use of sodium citrate buffer under closed-loop operation as a robust electrolyte for the electrode streams that also eliminates the waste they would otherwise generate.

Declaration of competing interest

The authors declare no competing financial interest.

Acknowledgments

This research was supported by a grant from Mitsubishi Heavy Industries Limited. The authors thank the Center for Environmental Health Sciences (CEHS) for the use of ICP–MS. MAA also acknowledges Dr. Hannes Grobe at the Alfred Wegener Institute in Germany for permitting adaptation of part of the graphical abstract.

References

[1] A.G. Dickson, C. Goyet, Handbook of Methods for the Analysis of the Various Parameters of the Carbon Dioxide System in Sea Water. Version 2, tech. rep. Oak Ridge National Lab., TN (United States), 1994.
[2] Q. Schiermeier, Water: Purification with a Pinch of Salt, (2008).
[3] H. Wang, Low-energy desalination, Nat. Nanotechnol. 13 (4) (2018) 273.
[4] M.A. Shannon, P.W. Bohn, M. Elimelech, J.G. Georgiadis, B.J. Marinas, A.M. Mayes, Science and technology for water purification in the coming decades, Nanoscience and Technology: A Collection of Reviews from Nature Journals, World Scientific, 2010, pp. 337–346.
[5] S.A. Kalogirou, Seawater desalination using renewable energy sources, Prog. Energy Combust. Sci. 31 (3) (2005) 242–281.
[6] D. Deng, W. Aouad, W.A. Braff, S. Schlumpberger, M.E. Suss, M.Z. Bazant, Water purification by shock electrodialysis: deionization, filtration, separation, and disinfection, Desalination 357 (2015) 77–83.
[7] D. Deng, E.V. Dydek, J.-H. Han, S. Schlumpberger, A. Mani, B. Zaltzman, M.Z. Bazant, Overlimiting current and shock electrodialysis in porous media, Langmuir 29 (52) (2013) 16167–16177.
[8] S. Schlumpberger, N.B. Lu, M.E. Suss, M.Z. Bazant, Scalable and continuous water deionization by shock electrodialysis, Environ. Sci. Technol. Lett. 2 (12) (2015) 367–372.
[9] J. Song, T. Li, L. Wright-Contreras, A.W.-K. Law, A review of the current status of small-scale seawater reverse osmosis desalination, Water Int. 42 (5) (2017) 618–631.
[10] J. Ayoub, R. Alward, Water requirements and remote arid areas: the need for small-scale desalination, Desalination 107 (2) (1996) 131–147.
[11] M.Z. Bazant, E.V. Dydek, D. Deng, A. Mani, Method and Apparatus for Desalination and Purification, (Aug. 12 2014) US Patent 8,801,910.
[12] M.Z. Bazant, E.V. Dydek, D. Deng, A. Mani, Desalination and Purification System, (Apr. 7 2015) US Patent 8,999,132.
[13] K.M. Conforti, M.Z. Bazant, Continuous ion-selective separations by shock electrodialysis, AIChE J. (2019) e16751.
[14] E.V. Dydek, B. Zaltzman, I. Rubinstein, D. Deng, A. Mani, M.Z. Bazant, Overlimiting current in a microchannel, Phys. Rev. Lett. 107 (11) (2011) 118301.
[15] A. Mani, M.Z. Bazant, Deionization shocks in microstructures, Phys. Rev. E. 84 (6) (2011) 061504.
[16] A. Mani, T.A. Zangle, J.G. Santiago, On the propagation of concentration polarization from microchannel- nanochannel interfaces Part I: analytical model and characteristic analysis, Langmuir 25 (6) (2009) 3898–3908.
[17] T.A. Zangle, A. Mani, J.G. Santiago, On the propagation of concentration polarization from microchannel- nanochannel interfaces Part II: numerical and experimental study, Langmuir 25 (6) (2009) 3909–3916.
[18] S. Nam, I. Cho, J. Heo, G. Lim, M.Z. Bazant, D.J. Moon, G.Y. Sung, S.J. Kim, Experimental verification of overlimiting current by surface conduction and electro-osmotic flow in microchannels, Phys. Rev. Lett. 114 (11) (2015) 114501.
[19] K.M. Conforti, Continuous Ion-selective Separation by Shock Electrodialysis, Ph.D. thesis Massachusetts Institute of Technology, February 2019.
[20] M.G. Ahunbay, S.B. Tantekin-Ersolmaz, W.B. Krantz, Energy optimization of a multistage reverse osmosis process for seawater desalination, Desalination 429 (2018) 1–11.
[21] A. Zhu, P.D. Christofides, Y. Cohen, Minimization of energy consumption for a two-pass membrane desalination: effect of energy recovery, membrane rejection and retentate recycling, J. Membr. Sci. 339 (1-2) (2009) 126–137.
[22] A. Azoulay, P. Garzon, M.J. Eisenberg, Comparison of the mineral content of tap water and bottled waters, J. Gen. Intern. Med. 16 (3) (2001) 168–175.
[23] H.-Y. Li, W. Ma, L. Wang, R. Liu, L.-S. Wei, Q. Wang, Inhibition of calcium and magnesium-containing scale by a new antiscalant polymer in laboratory tests and a field trial, Desalination 196 (1-3) (2006) 237–247.
[24] T.L. Brown, H.E. LeMay, B.E. Bursten, C.J. Murphy, P.M. Woodward, Chemistry: the Central Science, 12th, Pearson Education, 2012.
[25] D.R. Lide, CRC Handbook of Chemistry and Physics, 85th, CRC press, 2004.
[26] M. Alghoul, P. Poovanaesvaran, K. Sopian, M. Sulaiman, Review of brackish water reverse osmosis (BWRO) system designs, Renew. Sustain. Energy Rev. 13 (9) (2009) 2661–2667.
[27] N.C. Wright, et al., Justification for community-scale photovoltaic-powered electrodialysis desalination systems for inland rural villages in India, Desalination 352 (2014) 82–91.
[28] R. Zhao, S. Porada, P. Biesheuvel, A. Van der Wal, Energy consumption in membrane capacitive deionization for different water recoveries and flow rates, and comparison with reverse osmosis, Desalination 330 (2013) 35–41.